JGR Atmospheres

RESEARCH ARTICLE
10.1029/2021JD036075

Assessing Physical Relationships Between Atmospheric State, Fluxes, and Boundary Layer Stability at McMurdo Station, Antarctica

Mckenzie J. Dice[1,2,3] **and John J. Cassano**[1,2,3]

[1]Department of Atmospheric and Oceanic Sciences, University of Colorado Boulder, Boulder, CO, USA, [2]Cooperative Institute for Research in Environmental Sciences, University of Colorado Boulder, Boulder, CO, USA, [3]National Snow and Ice Data Center, University of Colorado Boulder, Boulder, CO, USA

Key Points:

- Self-organizing maps are used to examine the range of boundary layer conditions at McMurdo Station, Antarctica
- A strong seasonal cycle of boundary layer stability regimes exists, forced by varying net radiation and wind speed
- Low-level jets occur about 50% of the time below areas of enhanced stability aloft

Correspondence to:
M. J. Dice,
mckenzie.dice@colorado.edu

Citation:
Dice, M. J., & Cassano, J. J. (2022). Assessing physical relationships between atmospheric state, fluxes, and boundary layer stability at McMurdo Station, Antarctica. *Journal of Geophysical Research: Atmospheres*, *127*, e2021JD036075. https://doi.org/10.1029/2021JD036075

Received 19 OCT 2021
Accepted 6 JUL 2022

Abstract Observations at McMurdo Station, Antarctica from 24 November 2015 through 3 January 2017 were used to characterize the physical relationships between boundary layer stability and atmospheric state and fluxes. The basis of this analysis was self-organizing maps (SOMs), a neural network algorithm, used to identify the range of potential temperature profiles present in the twice-daily radiosonde data during the ARM (Atmospheric Radiation Measurement) West Antarctic Radiation Experiment (AWARE) campaign. The SOM identified profiles ranging from strongly stable to weakly stable regimes over the lowest 500 m of the atmosphere. It was found that in the winter (MJJA), moderate and strongly stable regimes occur most frequently (61%), while weakly stable regimes dominate in the summer (DJ, 83.4%). The mechanisms responsible for the dominance of different stability regimes in each season were analyzed to determine why these regimes occur with varying frequency throughout the year. This analysis found that wind speed variations and radiative cooling are responsible for the stability observed in the winter, radiative warming, as well as weaker wind speeds, are responsible for summer weak stability, and stability variations in the transition seasons (FMA, SON) are characterized by a change in sign of net radiation with increasing stability, as wind speed changes little across stability regimes. Low-level jets were observed to occur about 50% of the time below areas of enhanced stability aloft and were observed most frequently in the transition seasons. The boundary layer depth, as determined by the Bulk Richardson number, was found to decrease with increasing stability.

1. Introduction

Boundary layer stability in Antarctica has important implications for energy, momentum, and moisture fluxes between the atmosphere and surface, the vertical distribution of fluxes within the atmosphere, and processes such as turbulence generation (e.g., Chenge & Brutsaert, 2005; Lawrence & Balsley, 2013; Nigro et al., 2017). Boundary layer stability is important for the understanding of weather and climate in Antarctica and when evaluating weather and climate models. Low sun angle in the summer, polar night in winter, high albedo, and the cold, dry atmosphere of Antarctica all contribute to radiative cooling resulting in downward turbulent heat fluxes throughout most of the year and the creation of statically stable surface layers and frequent surface inversions (King & Turner, 1997). Wind shear plays an important role in shaping the boundary layer structure, as it is a source of mechanical mixing, which favors weakly stable boundary layers (Hudson & Brandt, 2005; Rodrigo & Anderson, 2013). The presence of low-level jets, a maximum in the wind speed profile, has important implications for vertical wind shear in the boundary layer which impacts the turbulent mixing within the boundary layer and the exchange of heat, moisture, and more (Tuononen et al., 2015). The effects of buoyancy and wind shear can be quantified using the bulk Richardson number, which identifies areas where turbulence is likely to occur (Stull, 1988). This paper will explore variability in near surface potential temperature profiles, which define boundary layer static stability, observed at McMurdo Station, Antarctica during the ARM (Atmospheric Radiation Measurement) West Antarctic Radiation Experiment (AWARE) campaign and examine the physical relationship between boundary layer static stability and the atmospheric state and fluxes.

Previous boundary layer studies in the Antarctic have relied on both tower and radiosonde observations. Hudson and Brandt (2005) used a 22 m instrumented tower on the East Antarctic plateau at the South Pole Amundsen-Scott Station (−90.0°S, 0.0°E) to characterize the temperature inversion and the factors that influence it. They observed inversion conditions between 2 and 22 m on the instrumented tower at the South Pole Amundsen-Scott Station

90% of the time in the winter, often exceeding 10 K, and 75% of the time in the summer, usually less than 1 K. They also found that the strongest winter inversions at the South Pole station occurred with winds of 3–5 m s^{-1}. Hudson and Brandt (2005) examined the downward longwave radiative flux and found that the temperature inversion strengths do not steadily decrease with increasing flux, but rather are constant when the downward longwave flux is less than 80 W m^{-2}. The inversion strength then begins to decrease with increasing flux above 80 W m^{-2} and approaches zero for a downward longwave flux above 150 W m^{-2}. An analysis of Amundsen-Scott South Pole Station daily radiosonde profiles from 2005 to 2018 found surface inversion layers were approximately 500 m thick throughout the year, but were shallower and less frequent in the summer (Xu et al., 2019).

Cassano et al. (2016) characterized the near-surface layer over the Ross Ice Shelf using two years of 10-minute time resolution data from a 30 m automatic weather station to analyze stability and wind using a neural network data analysis approach known as self-organizing maps (SOMs). It was found that stable conditions dominate at this site, occurring 83% of the time, and the strongest inversions over the 30 m height of the tower exceeded 25 K. This study also found a strong relationship between wind speed and inversion strength, with the strongest inversions occurring with wind speeds less than 4 m s^{-1}, and the strength of inversion decreasing substantially when the wind speed was above 4 m s^{-1}.

The South Pole Station is located on the high elevation Antarctic plateau, and thus is very different climatologically from coastal, low-lying locations (Cassano et al., 2016). Weaker surface inversions (Phillpot & Zillman, 1970) and warmer surface temperatures (Comiso, 1994) are characteristic of low-lying ice shelf and coastal regions, such as that of McMurdo Station, as opposed to the stronger inversions and colder temperatures observed in the studies mentioned above. Zhang et al. (2011) compared the frequency of surface-based inversions in the interior continent of Antarctica and along the Weddell Sea and East Antarctic coasts. They used two climate models and reanalysis data to show that the surface inversions in the Antarctic interior are more common than near the coasts.

Wind shear in the boundary layer has important implications for stability and turbulence. Jakobson et al. (2013) studied the effect of low-level jets (LLJs) by measuring wind speed profiles with a tethersonde system in the central Arctic Ocean from March–September 2007. They found that a LLJ was present 45% of the time, mostly occurring between 400 and 600 m above the surface. They observed average jet core wind speeds of 7.1 m s^{-1}. Comparing their work to that of Andreas et al. (2000) who analyzed LLJs over the Weddell Sea, Antarctica, they observed that the LLJ occurrence over the Arctic Ocean was far less than that observed over the Weddell Sea (80% of the time). Both papers used the bulk Richardson number to identify regions of turbulence in the atmosphere, and used the critical bulk Richardson number of 0.4, pointing to the literature regarding the choice of critical bulk Richardson number as somewhat arbitrary between values of 0.2 and 1.0 (Galperin et al., 2007). Additionally, Banta et al. (2007) found that strongly stable conditions were associated with large bulk Richardson numbers, primarily resulting from small values of wind shear.

The studies summarized in the previous paragraphs characterized the variability of near surface static stability and inversions across the Antarctic continent and determined what meteorological conditions are associated with different stability regimes. This paper will use over one year of radiosonde and surface flux data from a coastal Antarctic location to analyze the seasonal and annual variability in boundary layer stability and determine what meteorological conditions and fluxes are associated with differing stability. This analysis will use SOMs to identify the range of potential temperature profiles present in twice-daily radiosonde data from November 2015 to January 2017 during the AWARE campaign. The frequency of occurrence of each pattern and the relationship between the potential temperature profiles and wind speed, presence of LLJs, surface radiative fluxes, and Richardson numbers will be determined.

2. Data and Methods

2.1. Observational Data

The data used for this analysis are from the DOE AWARE campaign (Lubin et al., 2017, 2020; Silber et al., 2018), which took place at McMurdo Station and in West Antarctica from November 2015 to January 2017 (Figure 1a). Two datasets are used for the analysis presented here – radiosonde and flux observations. The basis of this analysis are observations made with Vaisala RS-92 radiosondes from 30 November 2015 through 3 January 2017 at the radiosonde launch site (−77.85°S, 166.66°E, at 10.1 m above sea level; Figure 1c). Radiosonde launches occurred twice per day, at approximately 1000 UTC and 2200 UTC. Surface radiative fluxes were observed from

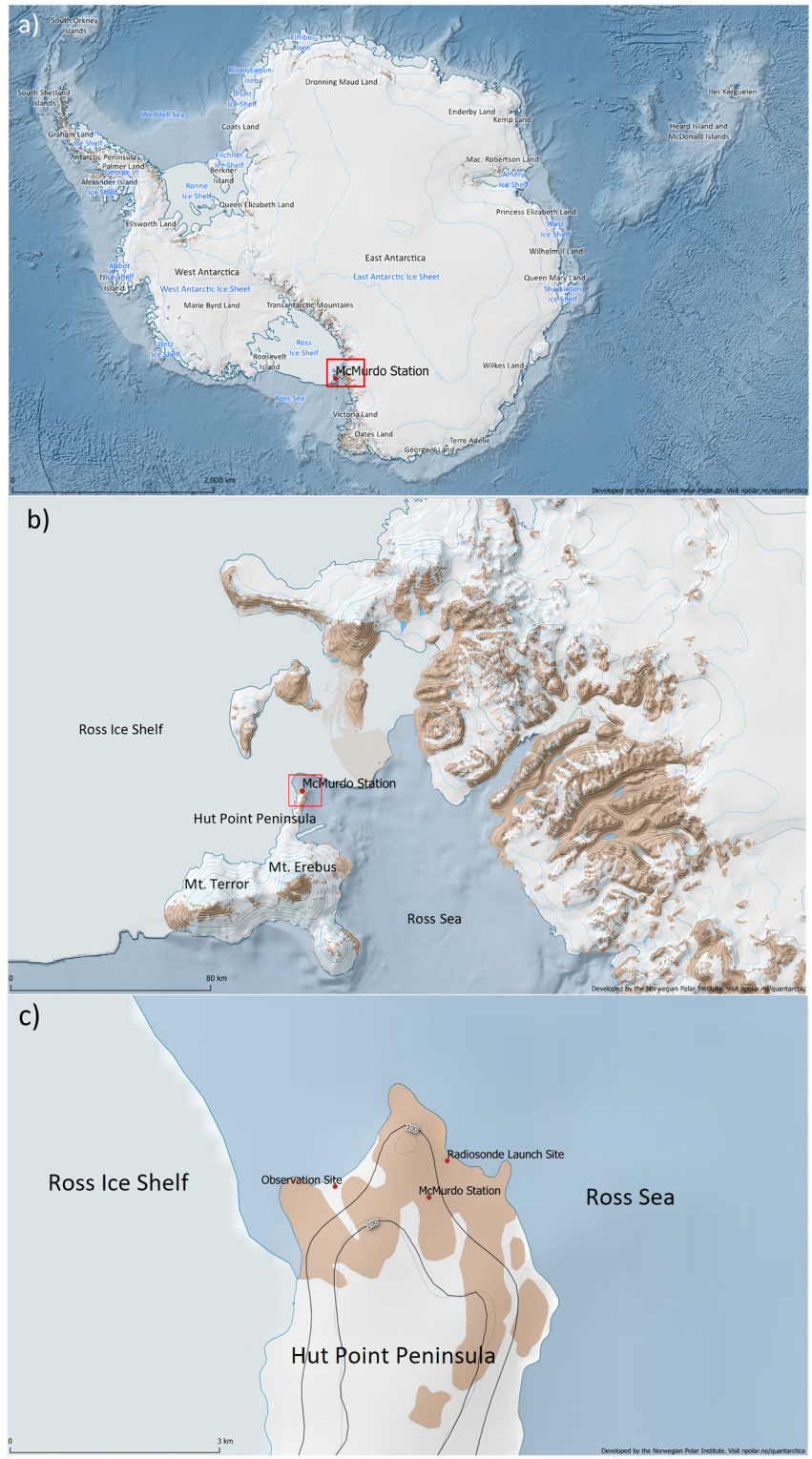

Figure 1. Maps of the Antarctic continent (a), Ross Island and adjacent areas (b), and the area near McMurdo Station (c). Red boxes in panels (a) and (b) show the area depicted in panels (b) and (c). Panel c shows the location of the AWARE radiosonde launch site and the observation site, where meteorological state and flux measurements were made. Maps courtesy of Quantarctica (Matsuoka et al., 2018).

24 November 2015 through 20 December 2016 at the observation site (−77.85°S, 166.73°E at 76.2 m above sea level; Figure 1c) which is a site several kilometers away from where the radiosondes were launched. In addition, the drift of the radiosonde as it ascends will result in the measured profiles not being vertical profiles at the launch site but instead a sloping profile that can drift ∼1 km during the time the radiosonde samples the boundary layer.

The area around McMurdo is characterized by steep, complex terrain that influences the wind flow and local meteorological conditions (Seefeldt et al., 2003; Figure 1b). As noted above the measurements used for the analysis presented here were taken at two different locations near McMurdo Station. It is important to note that the locations of the radiosonde launch site and the observation site (Figure 1c) have different meteorological conditions due to their different elevations and the locations on opposite sides of the Hut Point peninsula ridge. The observation site is located on the Ross Ice Shelf side of Hut Point peninsula, where there are higher wind speeds and colder temperatures, compared to the coastal location of the radiosonde launch site.

2.2. Methods

The goal of the research presented in this paper is to analyze variability in boundary layer stability, as defined by potential temperature profiles over the lowest 500 m of the atmosphere, and determine what meteorological conditions and fluxes are associated with the different boundary layer stability regimes. To determine the primary stability regimes that occur in the 787 AWARE radiosonde profiles, a data clustering technique known as SOMs is used.

The SOM analysis groups similar patterns, using an iterative training process, into a two-dimensional array, which is called the master SOM, or simply the SOM. The resulting array of SOM patterns represents a continuum of the different patterns present in the training data, in a way such that the squared difference between the training data and the patterns present in the SOM are minimized. Similar patterns in the SOM are located adjacent to each other on the two-dimensional array, while the most distinct patterns are on opposite sides of the SOM (Cassano et al., 2016). Here, the SOM is applied to 787 potential temperature profiles to provide information about the annual and seasonal boundary layer stability condensed into a smaller, yet comprehensive, visualization that represents the range of boundary layer states present in the training data.

In order to apply the SOM algorithm to the radiosonde data it was necessary to interpolate the radiosonde data onto a regular vertical grid. Thus, the radiosonde observations, starting at 10.1 m, were interpolated onto a vertical grid with 5-meter spacing from 15 m extending up to 1,000 m. A linear interpolation was used for the temperature, and the hypsometric equation was used to interpolate pressure. For this analysis, the SOM was initially trained on several height ranges (20–300 m, 20 to 500m, and 20–1,000 m) but it was found that using observations from 20 to 500 m was most appropriate since this height range includes the full depth of the boundary layer in most cases. It was decided to train the SOM with observations starting at 20 m due to the presence of anomalously warm temperatures at 10.1 and 15 m which are common when balloons are prepared in a heated environment and are not allowed time to equilibrate to the colder, outside environment before being released (Schwartz & Doswell, 1991).

For each sounding, potential temperature anomalies from the value at 20 m were calculated over the depth of the profile. The potential temperature anomaly was used to train the SOM because it preserves the shape of the profile and vertical gradients of potential temperature, which define the static stability, while ignoring the seasonal changes in potential temperature (Cassano et al., 2016).

The first step in training the SOM is choosing the size of the two-dimensional SOM array that will result from the training process (Cassano et al., 2015). A SOM with a small number of patterns shows stark differences between the profiles, whereas a SOM with a larger number of patterns shows more refined differences between the profiles. Smaller SOMs have the disadvantage that using only a small number of patterns can mean that small, yet critical, differences are lost in the more generalized patterns defined by the SOM. A disadvantage of a larger SOM is that it becomes more difficult to visualize and only a small number of cases correspond to each SOM pattern (Cassano et al., 2016). The goal of the SOM training is not to provide completely distinct patterns, but rather a range of patterns that vary smoothly across the states present in the training data (Cassano et al., 2015). For this analysis, 3×2 (6 patterns) to 7×6 (42 patterns) SOM sizes were trained, and it was found that a 5×4 SOM (20 patterns) best displayed the range of potential temperature profiles that were present in the 787 profiles used for training the SOM.

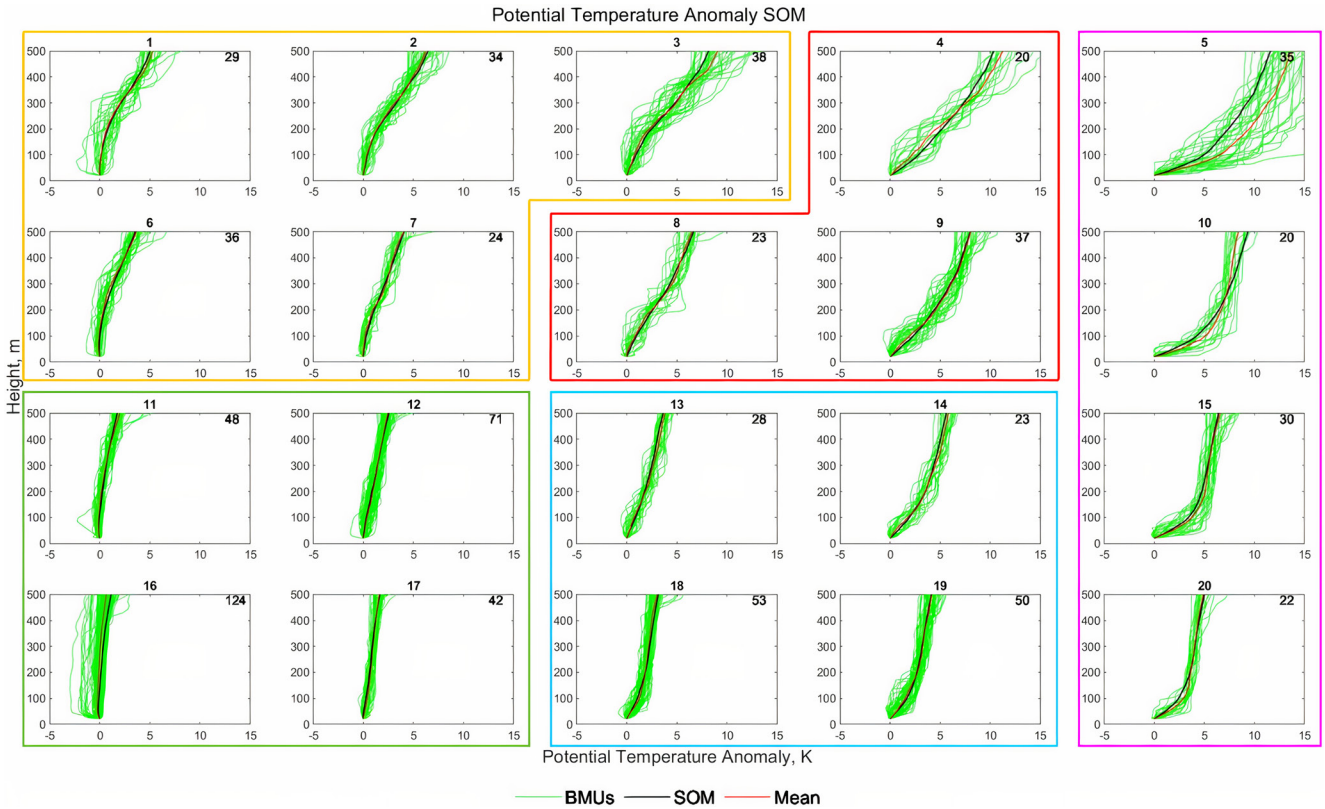

Figure 2. Potential temperature anomaly profiles from 20 to 500 m above ground level identified by the self-organizing map algorithm (black), the mean of all radiosonde observations corresponding to each SOM pattern (red), and all the individual radiosonde profiles that mapped to each pattern (green). The overall grid of patterns shown here is referred to as the master SOM. The numbers in the top right of each profile indicate the number of radiosonde profiles mapped to each regime, or the BMUs. The numbers above each SOM pattern are the pattern numbers. The colored outlines around the different SOM patterns indicate which stability regime the patterns correspond to: Weak Stability (WS): green, Weak Stability, Enhanced Aloft (WSEA): orange, Moderate Stability, Weak Aloft (MSWA): blue, Moderate Stability (MS): red, Strong Stability (SS): pink (Table 2).

Using the 20 master SOM patterns (Figure 2), individual profiles can be "mapped" to the SOM such that each individual profile is associated with one of the master SOM patterns (Cassano et al., 2016). This requires identifying a single master SOM pattern that is most similar to each individual profile in the training data such that the squared difference between the individual profile and the SOM pattern is minimized. Figure 2 shows all the radiosonde potential temperature profiles that were mapped to each pattern (thin green lines), indicating that the 20 trained SOM profiles (black lines) are largely representative of the profiles that map to each pattern.

Once the mapping is completed for every individual potential temperature anomaly profile in the training data set, a list of dates and times of all profiles that mapped to each SOM pattern is generated. The list of training data that maps to each SOM pattern are referred to as best matching units (BMUs). From the list of BMUs the frequency of occurrence of each pattern can be calculated. The BMUs can be analyzed on an annual or seasonal basis to identify what patterns of boundary layer structure occur at different times of the year.

The list of BMUs can also be used to composite other observations to each SOM pattern. The composited variables represent the range of conditions present when different potential temperature profiles were observed. Various statistics (mean, median, percentiles, etc.) can be calculated for each composited variable which allows for an analysis of the relationship between the SOM potential temperature profiles and other atmospheric properties, such as wind speed or radiative fluxes. The variables composited onto the SOM patterns can either be single-valued variables, such as surface wind speed or downwelling longwave radiation, or profile data, such as wind speed profiles. These relationships between the composited variables and the SOM potential temperature profile patterns will be a main focus of the results presented below.

The composited variables analyzed in this paper include the surface downwelling longwave radiation, surface net radiation, 20 m radiosonde wind speed. Wind speed, speed shear, total wind shear, and Richardson number profiles (Equation 1) are also composited. Atmospheric state variables composited onto the SOM were based on observations made at the time of each individual radiosonde launch. The radiation variables were averaged over a twelve-hour period prior to the radiosonde launch time before being composited onto the SOM. We choose to calculate twelve-hour averages so that the diurnal variability in solar radiation is removed from our analysis and the impact of aliasing of the diurnal cycle with observations made only twice per day is removed.

For the single-valued composites, the range of values that map to each SOM-identified stability regime is displayed as box and whisker plots. The profile plots show a mean or median profile for each variable for each SOM-identified stability regime. For both the box and whisker and profile plots the results are shown on an annual and seasonal basis.

Profiles of bulk Richardson number (R_B) were used to identify potentially turbulent layers within the lower atmosphere. The bulk Richardson number was calculated from the radiosonde data using:

$$R_B = \frac{g\Delta\theta\Delta z}{\bar{\theta}\left[(\Delta U)^2 + (\Delta V)^2\right]} \quad (1)$$

where g is acceleration due to gravity, θ is potential temperature, U is zonal wind, V is meridional wind, Δ indicates the difference between variables over the change in altitude Δz and the overbar indicates a mean potential temperature over each Δz. For this analysis Δz was 5 m.

3. Results

3.1. SOM Boundary Layer Stability Regimes and Seasonal Frequency of Occurrence

The SOM (Figure 2) trained with the AWARE radiosonde data depicts the range of potential temperature profiles observed near McMurdo Station, Antarctica. The variability of the static stability, as indicated by changes in the vertical gradient of potential temperature anomalies shown in the SOM, will be referred to in the rest of the paper simply as stability. As shown in Figure 2, the SOM profiles range from weak stability, with potential temperature increasing very slightly over the 500 m depth of the SOM pattern, in the bottom left, to increased stability, and greater vertical increase in potential temperature, moving towards the top right corner of the SOM.

To assist with interpretation of the individual SOM patterns, similar potential temperature profiles can be grouped together. These groups of SOM patterns will be referred to as stability regimes, or simply as regimes. The regimes were defined based on the vertical potential temperature gradient across the SOM-identified patterns (Table 1 and Figure A1 in Appendix A). Figure 3 shows the mean vertical potential temperature gradient and the mean potential temperature anomaly profile for each regime annually (top row) and seasonally (bottom three rows).

The description of each stability regime below will refer to the individual SOM patterns shown in Figure 2 and Figure A1 (Appendix A). The first regime exhibits weak stability (WS) throughout the depth of the profile, with potential temperature increasing only slightly over the 500 m depth analyzed, seen in the lower left corner of the SOM (patterns 11, 12, 16, and 17). The second regime, in the upper left portion of the SOM (patterns 1, 2, 3, 6 and 7), is characterized by weak stability near the surface with enhanced stability aloft, shortened to "weak stability, enhanced aloft", or WSEA in the remainder of the paper. The third regime, in the lower central portion of the SOM (patterns 13, 14, 18 and 19), is characterized by moderate stability at the surface with weak stability aloft (MSWA). There is also a regime characterized by moderate stability (MS) throughout the depth of the profile, seen in the upper central portion of the SOM (patterns 4, 8, and 9). Finally, there is a regime of strong stability (SS), seen in the rightmost column of the SOM (patterns 5, 10, 15, and 20). These stability regimes are summarized in Table 1.

Table 2 lists the annual and seasonal frequency of occurrence of the stability regimes. The frequency of occurrence for each pattern or regime in the SOM is calculated from the number of BMUs divided by the total number of observations, which was 787 profiles for the annual period, 234 profiles for the winter season (MJJA), 192 profiles for the summer season (DJ), and 361 profiles for the transition seasons (FMA and SON combined)

Table 1
Stability Regime Acronym, the Color Code Used to Outline Each Regime On Figures Throughout the Paper, the Master SOM Pattern Numbers From Figure 2 That Each Regime Is Made Up of, a Qualitative Description of What Is Seen in Each Regime, and the Magnitude of the Vertical Potential Temperature Gradient That Characterizes Each Regime

Stability regime	Figure color code	Pattern numbers	Description	Potential temperature gradient
Weak Stability (WS)	Green	11, 12, 16, and 17	Weak stability throughout the depth of the profile	−0.50 K (100 m)$^{-1}$ to +0.47 K (100 m)$^{-1}$ throughout profile depth
Weak stability, enhanced aloft (WSEA)	Orange	1, 2, 3, 6, and 7	Weak stability at the surface with enhanced stability aloft	20–200 m: −0.10 K (100 m)$^{-1}$ to +1.4 K (100 m)$^{-1}$
200–500 m: +1.1 K (100 m)$^{-1}$ to +2.0 K (100 m)$^{-1}$				
Moderate stability, weak aloft (MSWA)	Blue	13, 14, 18, and 19	Moderate stability at the surface with weak stability aloft	20–150 m: +1.2 K (100 m)$^{-1}$ to +1.9 K (100 m)$^{-1}$
150–500 m: +0.44 K (100 m)$^{-1}$ to +1.2 K (100 m)$^{-1}$				
Moderate stability (MS)	Red	4, 8 and 9	Moderate stability throughout the depth of the profile	+0.90 K (100 m)$^{-1}$ to +3.0 K (100 m)$^{-1}$ throughout profile depth
Strong stability (SS)	Pink	5, 10, 15, and 20	Strong stability at the surface	+0.50 K (100 m)$^{-1}$ to +8.8 K (100 m)$^{-1}$ throughout profile depth

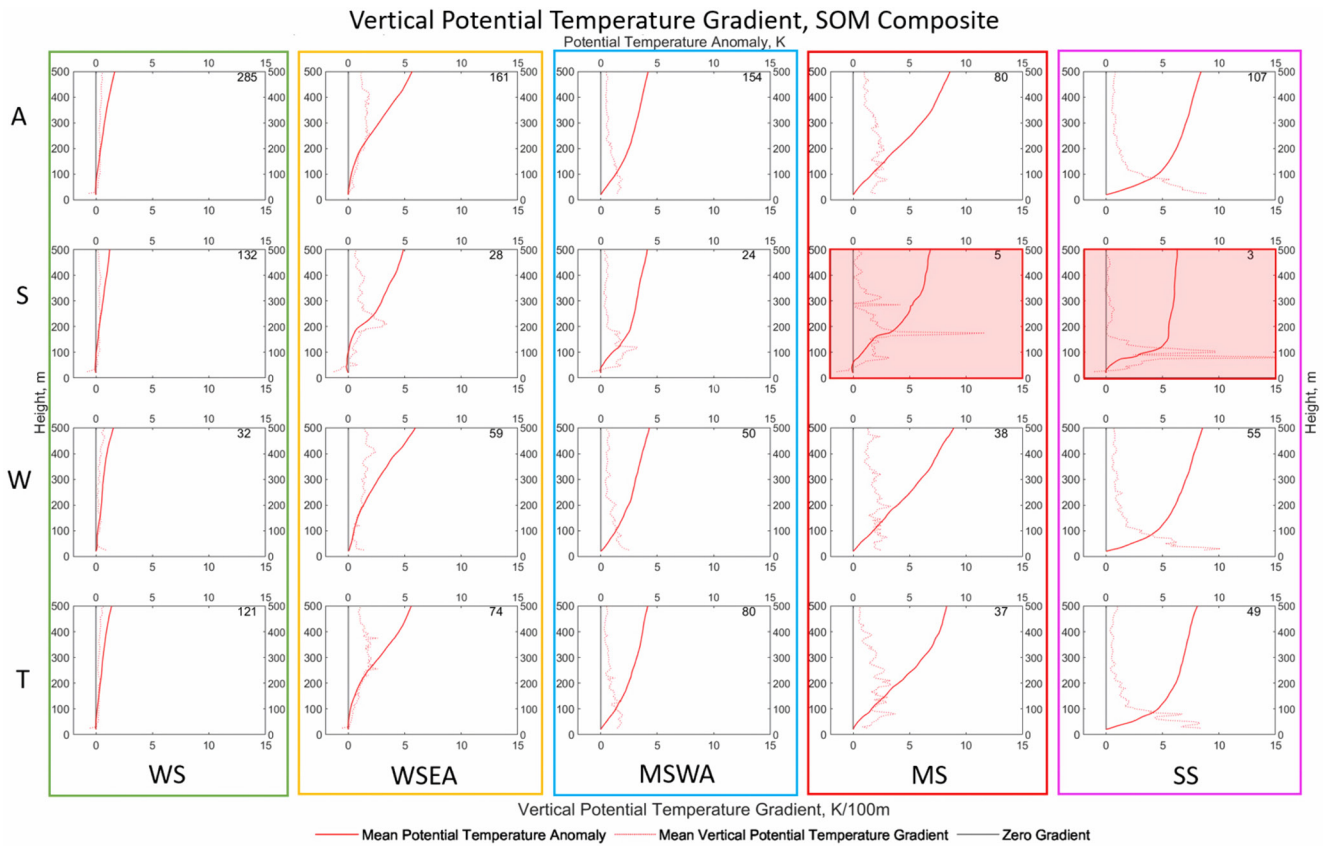

Figure 3. Mean potential temperature anomaly profile (solid red) and mean vertical potential temperature gradient profile (dotted red) shown annually (A) (top row), and for the summer (S), winter (W) and transition (T) seasons (second through fourth rows, respectively). A line of zero anomaly (gray) is also plotted. The numbers in the top right of each profile indicate the number of radiosonde profiles mapped to each regime, or the BMUs. Patterns with a red shade indicate that there were ten or fewer observations that mapped to that pattern.

Table 2
Frequency of Occurrence (%) for Each Stability Regime Annually and in Each Season and Number of BMUs (in Parenthesis)

Stability regime	Annual (frequency, BMUs)	Summer (frequency, BMUs)	Winter (frequency, BMUs)	Transition Seasons (frequency, BMUs)
WS	36.2% (285)	68.8% (132)	13.6% (32)	33.5% (121)
WSEA	20.4% (161)	14.6% (28)	25.3% (59)	20.5% (74)
MSWA	19.6% (154)	12.5% (24)	21.3% (50)	22.0% (80)
MS	10.1% (80)	2.6% (5)	16.2% (38)	10.2% (37)
SS	13.5% (107)	1.5% (3)	23.5% (55)	13.5% (49)

(Figure A2, Appendix A). The seasons were defined in this way to more accurately represent the annual cycle per previous definitions of Antarctic seasons (Cassano et al., 2016, Nigro et al., 2017).

On an annual basis the WS regime occurs more frequently (36.2%) than any other regime. The WSEA and MSWA regimes occur with intermediate frequencies (20.4% and 19.6%), and the MS and SS regimes occur the least frequently (10.1% and 13.5%, Table 2). In the winter the WSEA, SS, and MSWA regimes all occur more than 20% of the time while the WS regime occurs least frequently (13.6%). The moderate and strong stability regimes (MSWA, MS and SS) occur 61% of the time while weakly stable regimes occur 38.9% of the time in the winter. The summer season is dominated by the WS and WSEA regimes which occur 83.4% of the time. In contrast, the SS regime only occurs 1.5% of the time during the summer. The transition seasons exhibit a similar pattern to the annual period, with the WS regime occurring most frequently (33.5%), the WSEA and MSWA regimes occurring with intermediate frequencies (20.5% and 22.0%), and the MS and SS regimes occurring least frequently (10.2% and 13.5%).

The results in the previous two paragraphs can be qualitatively compared to the findings of the frequency of South Pole inversions observed by Hudson and Brandt (2005). They found that inversions occur in the winter 90% of the time and in the summer 75% of the time at the South Pole. The results for McMurdo Station indicate that the winter sees moderate to strong stability (MSWA, MS, and SS) 61% of the time, which occurs much less frequently in the summer (16.6%). This is consistent with summer inversions occurring less frequently as observed by Hudson and Brandt (2005) compared to in the winter, and with observations by Xu et al. (2019), who found shallower and less frequent summer temperature inversions. It should be noted that Hudson and Brandt (2005) made these observations at the South Pole Amundsen-Scott station, located in the interior continent, compared to the more coastal setting of McMurdo Station. The interior of the continent is colder, drier, and less windy, all features conducive to the formation of surface-based inversions (Zhang et al., 2011), which explains why inversion conditions occurred more frequently at the South Pole.

3.2. Atmospheric Forcing of Varying Stability Regimes

Variations in near surface stability result from the interplay of either heating or cooling of the atmosphere, due to varying surface energy fluxes or temperature advection, and mechanical mixing (Rodrigo & Anderson, 2013). It is expected that heating at the surface will lead to convection and weak stability while cooling at the surface will lead to the development of stable conditions (Phillpot & Zillman, 1970). Near surface wind speed will, in part, control the mechanical generation of turbulence with stronger winds leading to more turbulence and weakened near surface stability (Banta et al., 2007). Here, the effects of heating and cooling as well as mechanical mixing will be considered using composited variables of downwelling longwave radiation, net radiation, and wind speed.

3.2.1. Radiative Effects on Stability Regimes

Figure 4 shows box and whisker plots of the composited surface downwelling longwave radiation for each stability regime annually and seasonally. This figure, and subsequent box plot figures, is organized such that for the annual and seasonal periods the regime stability increases from left to right for each analysis period (indicated on the *x*-axis). The box plots show the median (horizontal red line), mean (middle red asterisk), 25th and 75th percentiles (limits of blue box), 10th and 90th percentiles (outer red asterisks), and the minimum and maximum values (whiskers) for the variable shown. Displayed in this way, these figures highlight how the composited variables vary as a function of the different stability regimes both annually and seasonally.

The largest median values of downwelling longwave radiation occur in the WS regime and decrease with increasing stability both annually and seasonally (Figure 4). A decrease is seen in winter in median downwelling longwave radiation from the WS to SS regimes from 186 W m $^{-2}$ to 139 W m $^{-2}$. Summer median downwelling longwave radiation is largest for the WS regime (228 W m^{-2}) and about 10–20 W m^{-2} less in the WSEA (220 W m^{-2}) and MSWA (212 W m^{-2}) regimes. Similar to in winter, there is a decrease in median downwelling longwave radiation from the WS to SS regime in the transition seasons (decrease from WS to SS from 202 W m^{-2} to 155 W m^{-2}). The reduction in downwelling longwave radiation with increasing stability is consistent with

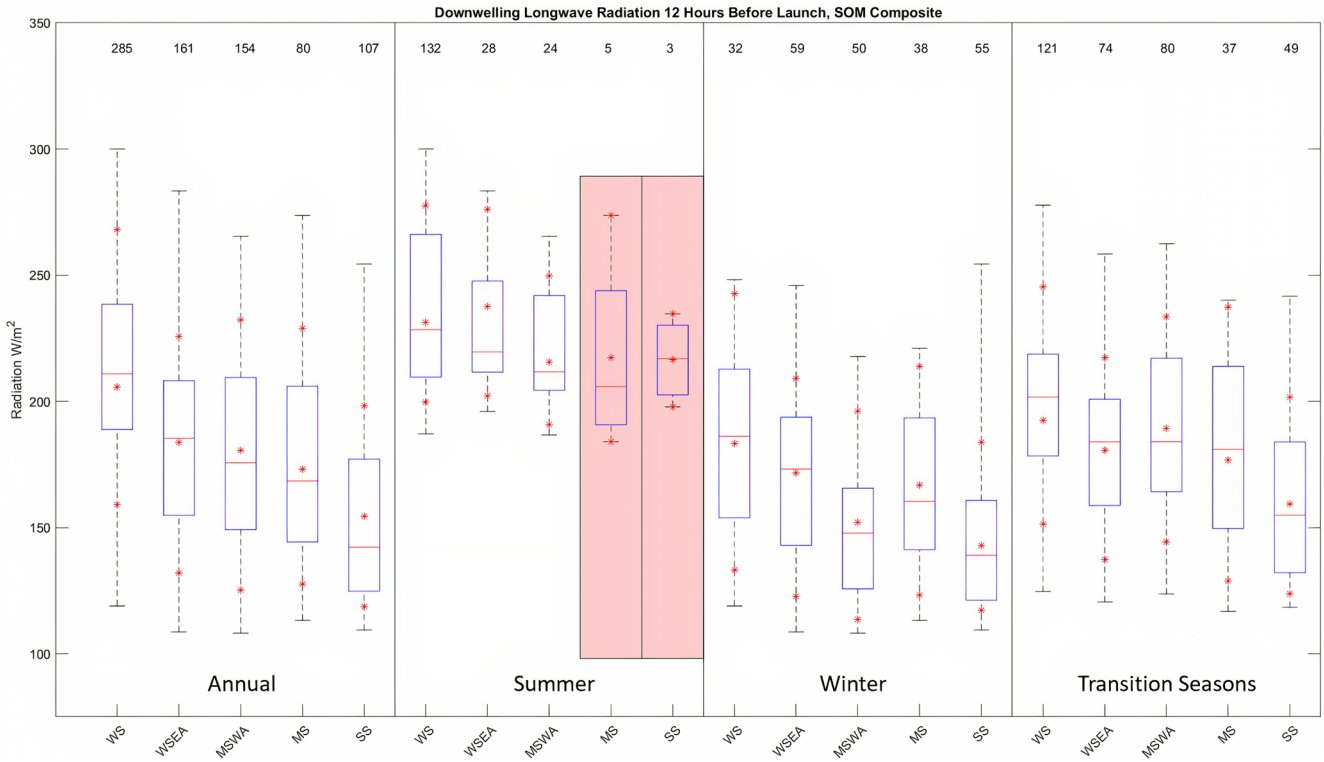

Figure 4. Median downwelling longwave radiation (red horizontal line), 25th and 75th percentiles (edges of blue boxes), mean downwelling longwave radiation (center red star), 10th and 90th percentiles (outer red stars), and minimum and maximum (whiskers) for each stability regime (WS, WSEA, MSWA, MS and SS) for annual and seasonal periods. The numbers at the top indicate the number of radiosonde profiles mapped to each regime. Patterns with a red shade indicate that there were ten or fewer observations that mapped to that pattern.

reduced surface radiative warming from the atmosphere leading to the development of enhanced near surface stability. Hudson and Brandt (2005) found that strong inversions at the South Pole station occur less frequently with increasing downward longwave radiation consistent with the changes in downwelling longwave radiation as a function of stability seen in Figure 4.

In order to determine what impact variations in net radiation have on the stability regimes the surface net radiation is analyzed as a function of stability regimes (Figure 5). The net radiation is negative in the winter, indicating net surface cooling, and positive in the summer, indicating net surface heating, for all regimes. This is surprising given that both weak and moderate to strong stability regimes occur in all seasons, thus, we would expect that the sign of net radiation would change across these stability regimes. However, the positive net radiation in the summer is consistent with the dominant weak stability in this season, and in the winter, the dominance of the MSWA, MS, and SS regimes are consistent with the observed negative net radiation. The expected change in sign from positive net radiation associated with weak stability and negative net radiation associated with strong stability is observed in the transition seasons.

In winter the median net radiation decreases from the WS to SS regime (-27 W m^{-2} to -55 W m^{-2}), with negative net radiation seen across all regimes, even the WS and WSEA regimes. This suggests that the weak stability in these regimes is due to another mechanism other than surface heating. There is little difference in median net radiation across WS and WSEA (178 W m^{-2} and 171 W m^{-2} respectively) regimes in the summer, with higher net radiation in the MSWA regime (209 W m^{-2}). Surface radiative heating in summer favors formation of weak stability regimes that dominate at this time of year, and limits the ability of the stronger stability classes to develop. The median net radiation in the transition seasons decreases from WS to SS (50 W m^{-2} to -24 W m^{-2}), but at this time of year, in contrast to winter and summer, the WS and WSEA regimes are characterized by positive net radiation which would help generate convection and lead to weak stability in the boundary layer, and the SS regime exhibits negative net radiation, favoring the formation of this regime.

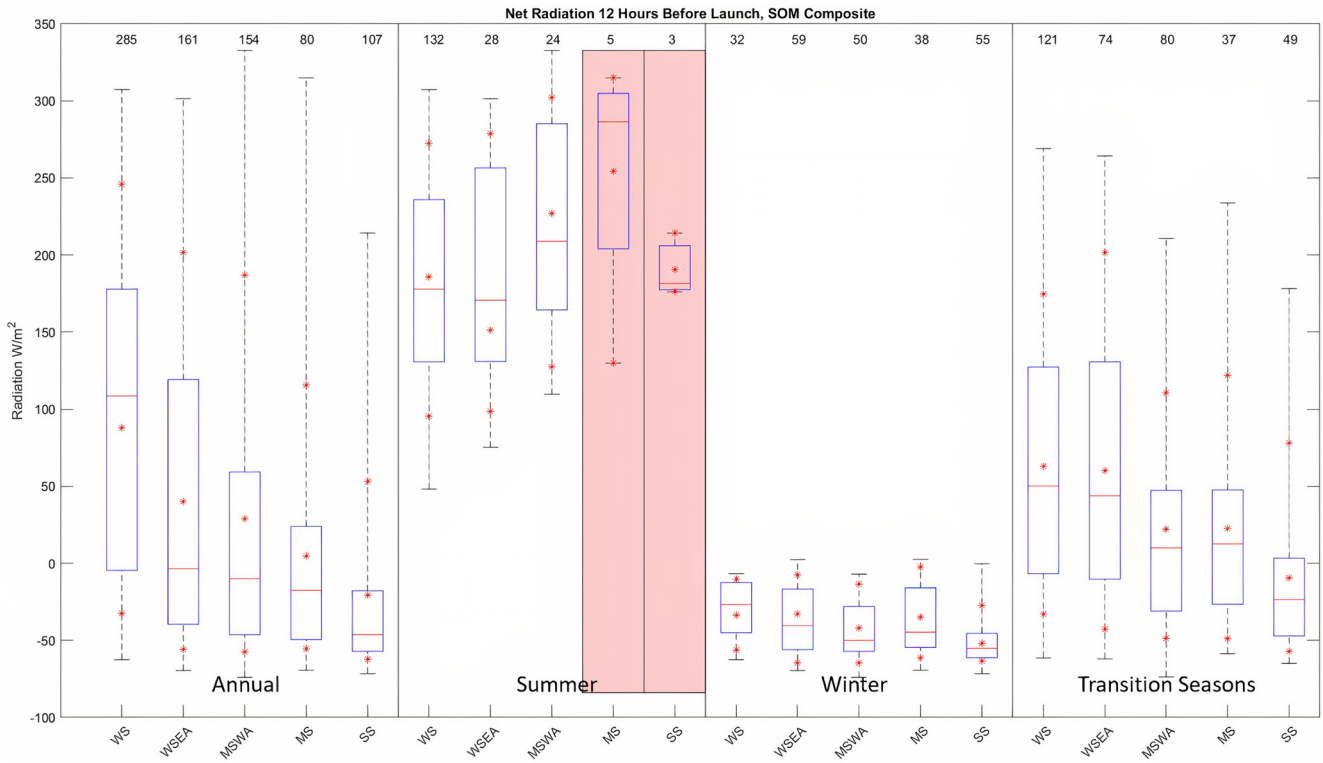

Figure 5. Median net radiation (red horizontal line), 25th and 75th percentiles (edges of blue boxes), mean net radiation (center red star), 10th and 90th percentiles (outer red stars), and minimum and maximum (whiskers) for each stability regime (WS, WSEA, MSWA, MS and SS) for annual and seasonal periods. The numbers at the top indicate the number of radiosonde profiles mapped to each regime. Patterns with a red shade indicate that there were ten or fewer observations that mapped to that pattern.

3.2.2. Mechanical Mixing Effects on Stability Regimes

Rodrigo and Anderson (2013) note that differences in radiation primarily drive variation in stability near the surface, which can then be modified by mechanically generated turbulence. It is expected that stronger winds and thus larger wind shear will result in more turbulence and mechanical mixing and lead to reduced stability (Cassano et al., 2016). Here the 20 m radiosonde wind speed is used as a proxy to indicate mechanical generation of turbulence at the surface to explore the relationship between turbulence and the SOM-identified stability regimes.

Figure 6 shows the box and whisker plots of the composited 20 m radiosonde wind speed for each stability regime. In the winter, the median wind speeds in the MSWA (1.9 m s^{-1}), MS (1.6 m s^{-1}) and SS (1.2 m s^{-1}) regimes are less than in the WS (4.0 m s^{-1}) and WSEA (4.1 m s^{-1}) regimes, consistent with weaker mechanical mixing in the moderate and strong stability regimes. The stronger 20 m wind speeds in the WS and WSEA regimes in the winter, indicate they are likely driven by mechanical mixing since the results in Figure 5 indicated negative net radiation for these regimes in winter.

In the summer the median 20 m wind speed is 3.7 m s^{-1} in the WS regime and 5.9 m s^{-1} in the WSEA regime, and these moderate wind speeds are consistent with the weak stability seen. The moderate median wind speeds and mechanical turbulence in the MSWA, MS, and SS regimes is inconsistent with the moderate near-surface stability, particularly in light of the positive net radiation seen for these regimes in summer (Figure 5).

The wind speed in the transition seasons show slightly less variability across the different stability regimes (3.5 m s^{-1}–5.8 m s^{-1}) compared to the winter season. It would be expected that weaker winds would favor strong to moderate stability near the surface, but this is not the case for the MSWA and MS regimes with wind speeds of 4.2 m s^{-1} and 5.8 m s^{-1}, respectively. With the moderate 20 m wind speed and positive net radiation, the MSWA and MS regimes are difficult to explain. Some potential explanations for this will be given in Section 3.2.3. To further demonstrate the dependence of the regime formation mechanisms in the transition seasons, the 20 m wind

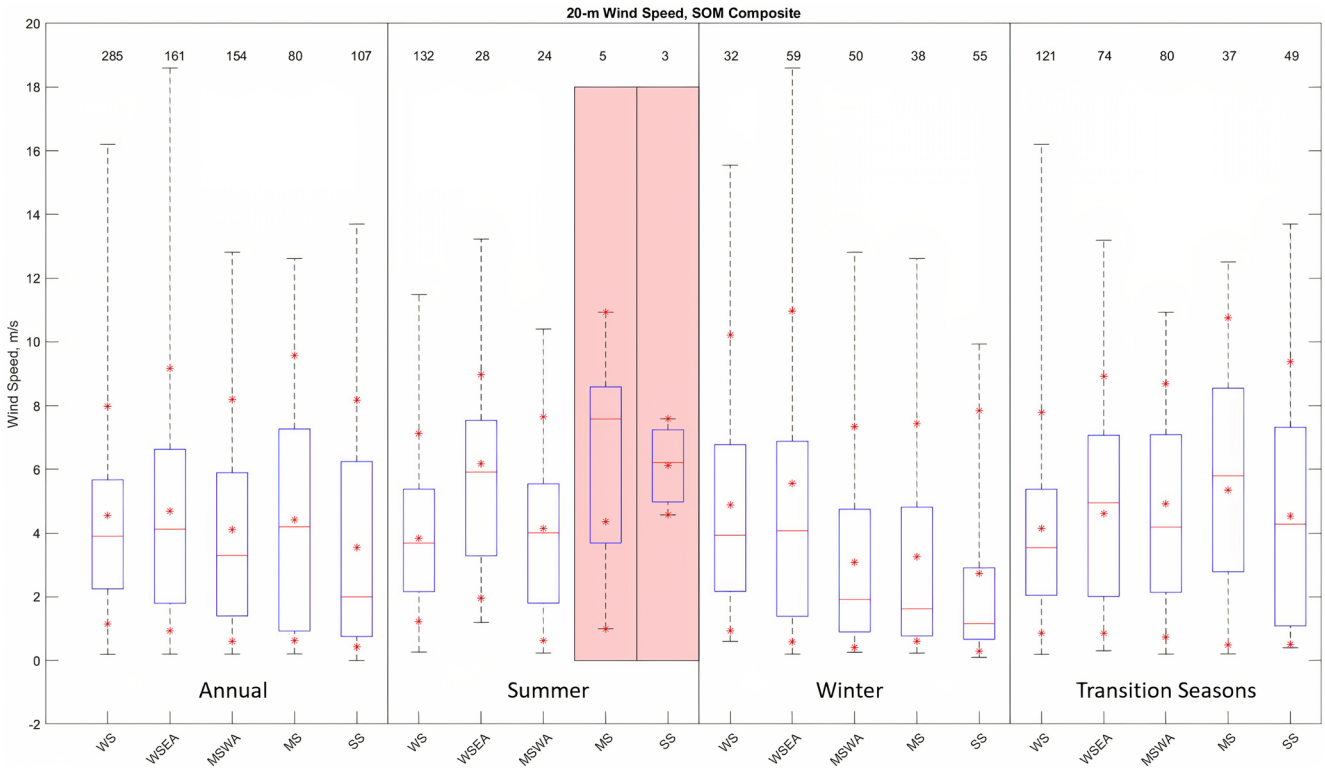

Figure 6. Median 20 m wind speed (red horizontal line), 25th and 75th percentiles (edges of blue boxes), mean 20-meter wind speed (center red star), 10th and 90th percentiles (outer red stars), and minimum and maximum (whiskers) for each stability regime (WS, WSEA, MSWA, MS and SS) for annual and seasonal periods. The numbers at the top indicate the number of radiosonde profiles mapped to each regime. Patterns with a red shade indicate that there were ten or fewer observations that mapped to that pattern.

speeds in the WS regime (3.5 m s^{-1}) and in the SS regime (4.3 m s^{-1}) are similar, so the negative median net radiation in the SS regime must be what allows strong stability to develop in the transition seasons, despite this lack of difference in mechanical forcing between the most extreme regimes. However, when comparing the SS regime in the transition seasons to the WS regime in the winter characterized by even more negative net radiation and similar wind speed, it is interesting that the SS regime is still able to form with the observed conditions in the transition seasons. Thus, this result is surprising, and, similar to the MSWA and MS regimes in the transition seasons, there may be other forcing mechanisms that are causing the formation of the SS regime.

Hudson and Brandt (2005) observed the strongest inversions at the South Pole Amundson-Scott station occurred when the wind speeds in the winter were between 3 and 5 m s^{-1}. Similarly, Riordan (1977) found that the strongest inversions throughout the year occurred when the wind speed was between 3 and 6 m s^{-1}. Cassano et al. (2016) found that the strongest inversions above the Ross Ice Shelf occurred with winds less than 4 m s^{-1}. In this analysis, it was found that the strongest inversions (the SS regime) occur when the median wind speed is between 1.2 and 4.3 m s^{-1}. Our results are generally consistent with these previous studies, although both Hudson and Brandt (2005) and Riordan (1977) note slightly stronger wind speeds for strong inversion conditions than we find for the SS regime at McMurdo and this may be due to the fact that they were analyzing inversions on the high polar plateau where radiative cooling is stronger.

3.2.3. Summary of Atmospheric Forcing of Stability Regimes

The winter is the most clearly explained season for variations in boundary layer stability in response to changes in net radiation and wind speed. Mechanically generated turbulence is responsible for the WS and WSEA regimes occurring in the winter since the negative net radiation observed for these regimes in winter would result in stronger near surface stability. It is also worth noting that increased downwelling longwave radiation and less negative net radiation in the WS regime is a potentially important aspect of these regimes since this lessens the amount of surface cooling, which would result in decreased stability. The MSWA, MS, and SS regimes are

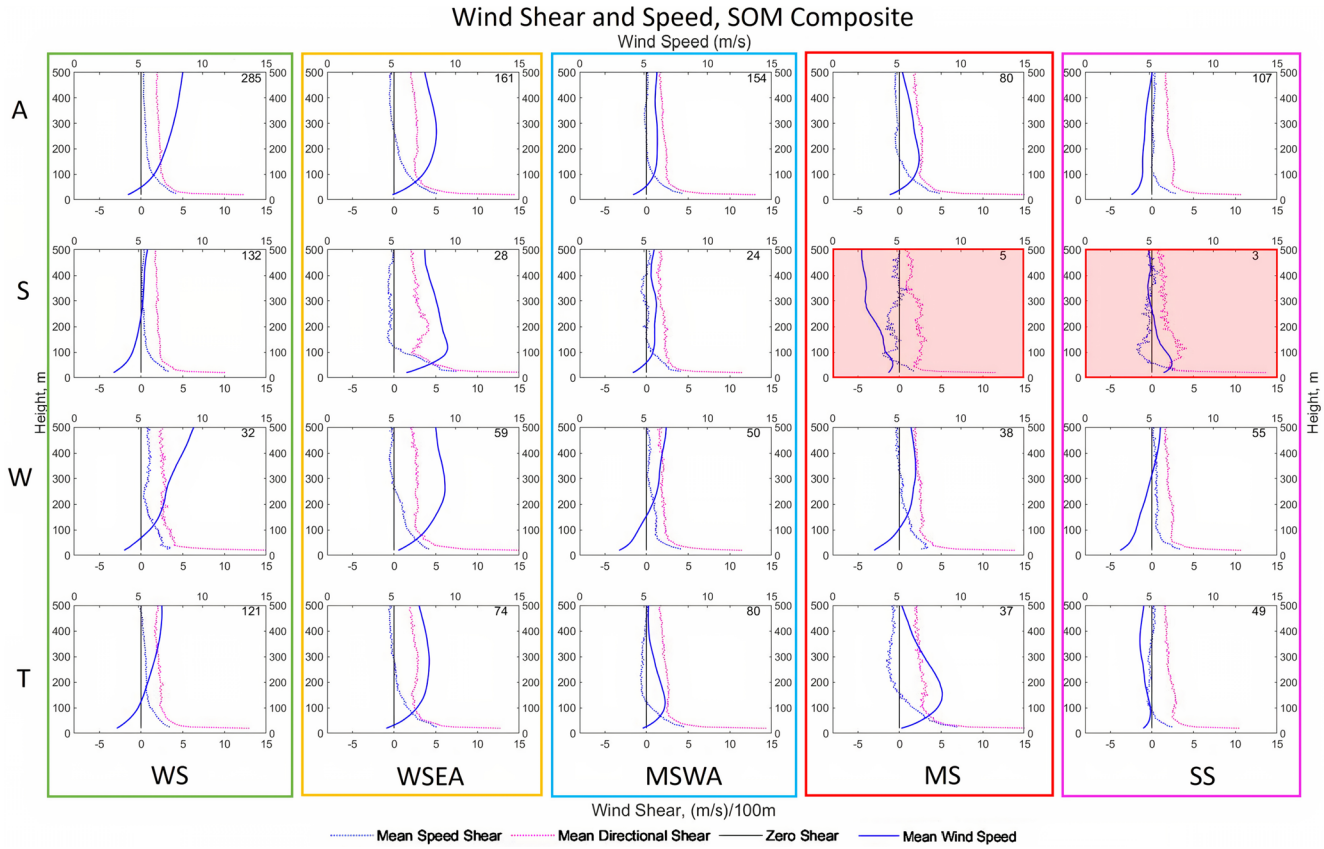

Figure 7. Mean wind speed shear profile (dotted blue), mean potential temperature anomaly profile (solid red line), and mean wind speed profile (solid blue), and a line of zero shear (gray) for each stability regime (WS, WSEA, MSWA, MS, and SS) annually (A) (top row), and for the summer (S), winter (W), and transition (T) seasons (second through fourth rows, respectively). The numbers in the top right of each profile indicate the number of radiosonde profiles mapped to each regime. Patterns with a red shade indicate that there were ten or fewer observations that mapped to that pattern. The wind speed and potential temperature anomaly are associated with the top *x*-axis, and the shear profiles are associated with the bottom *x*-axis.

characterized by much weaker winds and slightly more negative net radiation, which contribute to the formation of these regimes in the winter.

In the summer, positive net radiation is largely responsible for the formation of the WS and WSEA regimes, with mechanical mixing (Figure 6) aiding in the high frequency of these weak stability regimes in the summer. The MSWA regime, which occurs 12.5% of the time, and the MS and SS regimes, which occur only 4.1% of the time, are more difficult to explain. For all three of these regimes, the positive net radiation (Figure 5) and moderate 20 m wind speeds (Figure 6) are inconsistent with moderate to strong stability. There are several possibilities for the formation of these regimes in summer. The close proximity of sea ice in McMurdo Sound to the radiosonde launch site could have an effect on near surface stability. In the summer, the mostly snow free ground at McMurdo station would support convection and weak stability, but if the low-level wind blows onshore from the sea ice, cold air would infiltrate near the surface, resulting in the stable profiles that are observed. This, or another source of low-level cold air advection, which weakens with height could result in moderate or strong low-level stability. Alternatively, warm air advection that strengthens with height could result in enhanced low-level stability.

Radiative effects play the main role in shaping the stability of the WS, WSEA and SS regimes in the transition seasons, with positive net radiation characterizing the WS and WSEA regimes and negative net radiation found for the SS regime (Figure 5). The forcing for the MS and MSWA regimes in the transition seasons is less clear, since the median net radiation is just above zero meaning that more than half of the cases in these regimes have positive net radiation. This radiative heating of the surface for these cases is inconsistent with the formation of moderate near surface stability. It is possible that the MSWA and MS cases with positive net radiation could form as a result of differential temperature advection (similar to the summer cases), or as a result of a stable profile

advecting from over the Ross Ice Shelf or sea ice. The strong near surface winds seen in this regime suggest a potentially more active synoptic situation, which would be consistent with strong temperature advection.

For some of the regimes that are more difficult to explain, such as the stronger stability in the summer and the MS and MSWA regimes in the transition seasons, it may be possible that the different location of the radiosonde launch site compared to the location of the observation site several kilometers away contributes to some of the mismatch between regime stability and the radiation observations. The complexities of the local terrain may also help explain the regimes that do not have clear formation mechanisms. Further, the fact that the radiosonde does not observe a vertical profile and may drift up to ∼1 km from the launch site over the portion of the atmosphere analyzed here may also contribute to some of the regimes which have unclear formation mechanisms.

To investigate the possible impact of varying wind direction on the different stability regimes, the mean wind direction profiles and the BMUs of the wind direction profiles for each stability regime and season are shown in Figure A3 (Appendix A). The large scatter in the individual wind direction profiles indicates that the mean profiles shown should be viewed with caution. For example, the backing shown in the mean wind direction profile in the MS regime in the transition seasons is not representative of the individual wind direction BMU profiles, where largely veering occurs. Below we discuss the mean profiles and the dominant wind direction, but it should be noted that most of the regimes show a secondary preferred wind direction that is not quite 180° opposite the primary wind direction discussed below.

In the summer, the wind direction is largely consistent near the surface (easterly) and throughout the depth of the profile (turning to the southeast with height). The winter is also largely characterized by easterly near-surface winds that turn to southeasterly aloft but in the winter the change in wind direction to southeasterly occurs more sharply. For the WSEA regime the shift to southeasterly winds occurs at around 150 m and near 300 m in the MSWA, MS, and SS regimes, which corresponds to the height of the local topography. In the transition seasons, the wind direction pattern is largely similar to the summer season, with easterly near-surface winds turning to the southeast with height, but the MS regime exhibits a more northeasterly mean near-surface wind direction, which turns to the north with height, backing, unlike any of the other wind direction profiles, although this mean backing appears to be an artifact of averaging the two varying wind direction regimes and is not reflected in most of the individual wind profiles for the MS stability regime.

The wind direction profiles in Figure A3 (Appendix A) show that near the surface, mean easterly winds from the nearby Ross Ice Shelf could advect air masses from over the ice into the area where the radiosondes are launched. Then, for the most part, the radiosondes can be advected to the west away from the radiosonde launch site over the adjacent sea ice or open water of McMurdo Sound (the Ross Sea, Figure 1c). With some of the more stable profiles such as the MS and SS regimes in the summer and the MSWA and MS regimes in the transition seasons, this may result in warmer temperatures observed near the surface above the ice-free ground on Hut Point Peninsula and then colder temperatures aloft over the McMurdo Sound, but this is not what is seen in the stability profiles (Figure 3). Rather than the drift of the radiosonde over McMurdo Station affecting the stability of the observed profiles, the moderate and strong stability seen in the summer and transition seasons are likely dominated by low-level winds blowing onshore from the sea ice, another source of low-level cold air advection, which weakens with height, or warm air advection that strengthens with height.

3.3. Atmospheric Conditions Associated With Varying Stability Regimes

The analysis shown above has focused on how radiative fluxes and mechanically generated turbulence shape the stability profiles seen in the different regimes. Here we will use the depth of mechanical mixing and the bulk Richardson number to identify what layers of the atmosphere may or may not be turbulent based on how stability and wind shear profiles vary in the different regimes (Zilitinkevich & Baklanov, 2002).

Figure 7 shows profiles of wind speed (top x-axis), wind speed shear (bottom x-axis), and mean potential temperature anomaly (top x-axis) to allow comparison of wind and stability features throughout the depth of the boundary layer. In the regime mean wind profiles (Figure 7) low-level wind maxima are present in the WSEA regime for each season and in the MSWA, MS, and SS regimes in the transition seasons. For all the low-level wind maxima the wind shear is larger below the maximum than above the maximum. This means that the low-level wind speed maximum will enhance shear and mixing near the surface beyond what would occur if no wind speed maximum

Table 3
Frequency (%) and Number (in Parenthesis) of LLJ Occurrence in Each Regime for Each Season

	WS	WSEA	MSWA	MS	SS
Annual (frequency, BMUSs)	X	53% (85)	25% (38)	34% (27)	22% (24)
Summer (frequency, BMUSs)	X	50% (14)	X	X	X
Winter (frequency, BMUSs)	X	56% (33)	X	X	X
Transition Seasons (frequency, BMUSs)	X	51% (38)	48% (38)	73% (27)	49% (24)

Note. An X indicates that no LLJs were identified for that regime and season.

was present, while the shear above the maximum can extend the depth of mechanical mixing beyond what would be seen without a low-level wind speed maximum.

We suspect that there are two possible mechanisms that cause these low-level wind maxima to form. For the WSEA regime, we hypothesize that the enhanced stability aloft acts as a "lid" on the lowest portion of the atmosphere causing winds approaching the Ross Island terrain to be funneled between the terrain and the enhanced stability aloft, resulting in an acceleration of low-level flows (Tuononen et al., 2015). This, combined with friction near the surface, results in a wind speed maximum just below the region of enhanced stability aloft and the formation of the low-level wind maxima observed across all seasons in the WSEA regime. The presence of this low-level wind maximum also helps explain the stronger near-surface wind speeds seen in the WSEA regime seasonally and annually (Figure 6).

In contrast to the situation in the WSEA regime where the low-level wind maximum is located below the level of enhanced stability, the low-level wind maximum occurs within the layer of enhanced stability near the surface in the MSWA, MS, and SS regimes in the transition season. We hypothesize that these low-level wind maxima form as a result of the horizontal temperature gradients in these regimes, created by the presence of an inversion over the sloping terrain of Ross Island, which results in a southeasterly thermal wind parallel to the terrain of Hut Point Peninsula (Figure 1c) that is strongest near the surface and decreases with height through the inversion. Above the inversion the large-scale meridional temperature gradient results in a westerly thermal wind. The southeasterly thermal wind in the inversion layer increases the prevailing easterly surface wind (Figure A3, Appendix A) through the depth of the inversion. Friction near the surface and the westerly thermal wind above the inversion results in a wind speed maximum within the layer of enhanced stability.

The analysis above identified low-level wind speed maxima in the mean wind speed profiles, but the frequency of low-level jet (LLJ) occurrence can also be examined in these regimes. While Jakobson et al. (2013) and Andreas et al. (2000) used Stull's (1988) definition of LLJs, there are many other definitions used to identify LLJs (Baas et al., 2009; Bonner, 1968; Carroll et al., 2019; Parish, 2017; Tuononen et al., 2015). LLJs in this paper are defined following the first criterion of Baas et al. (2009): the maximum wind speed below 500 m is at least 2 m s^{-1}, and additionally the minimum wind speed above the jet core is at least 2 m s^{-1} lower than that in the jet core (Stull, 1988). Table 3 shows the frequency of occurrence of LLJs for each regime. In the WSEA regime, the LLJ is observed more than 50% of the time for all seasons, consistent with the low-level wind speed maxima seen in this regime for all seasons in Figure 7. In the MSWA, MS, and SS regimes, LLJs occur from 48% to 73% of the time in the transition seasons, with the highest frequency of LLJ occurrence in the MS regime. LLJs are not observed for any WS profiles in any season.

Jakobson et al. (2013) found that LLJs over the Arctic Ocean occurred within the temperature inversion in most cases, whereas in the results presented here the low-level wind maximum occurs below the enhanced stability in the WSEA regime, but within the layer of enhanced stability in the MS regime. Jakobson et al. (2013) compared their observed location of the LLJ with respect to the location of the inversion to another study, which observed LLJs above the region of enhanced stability, and also concluded that these differences in location of the LLJ in relation to the temperature inversion may be due to orographic effects.

The bulk Richardson number is the ratio of buoyant turbulence production or suppression to mechanical generation of turbulence by wind shear (Stull, 1988). Positive bulk Richardson numbers indicate stability acting to suppress turbulence, the degree to which this suppression is successful depends on the stability and wind shear strength. A higher positive bulk Richardson number indicates strong stability and/or weak wind shear, whereas

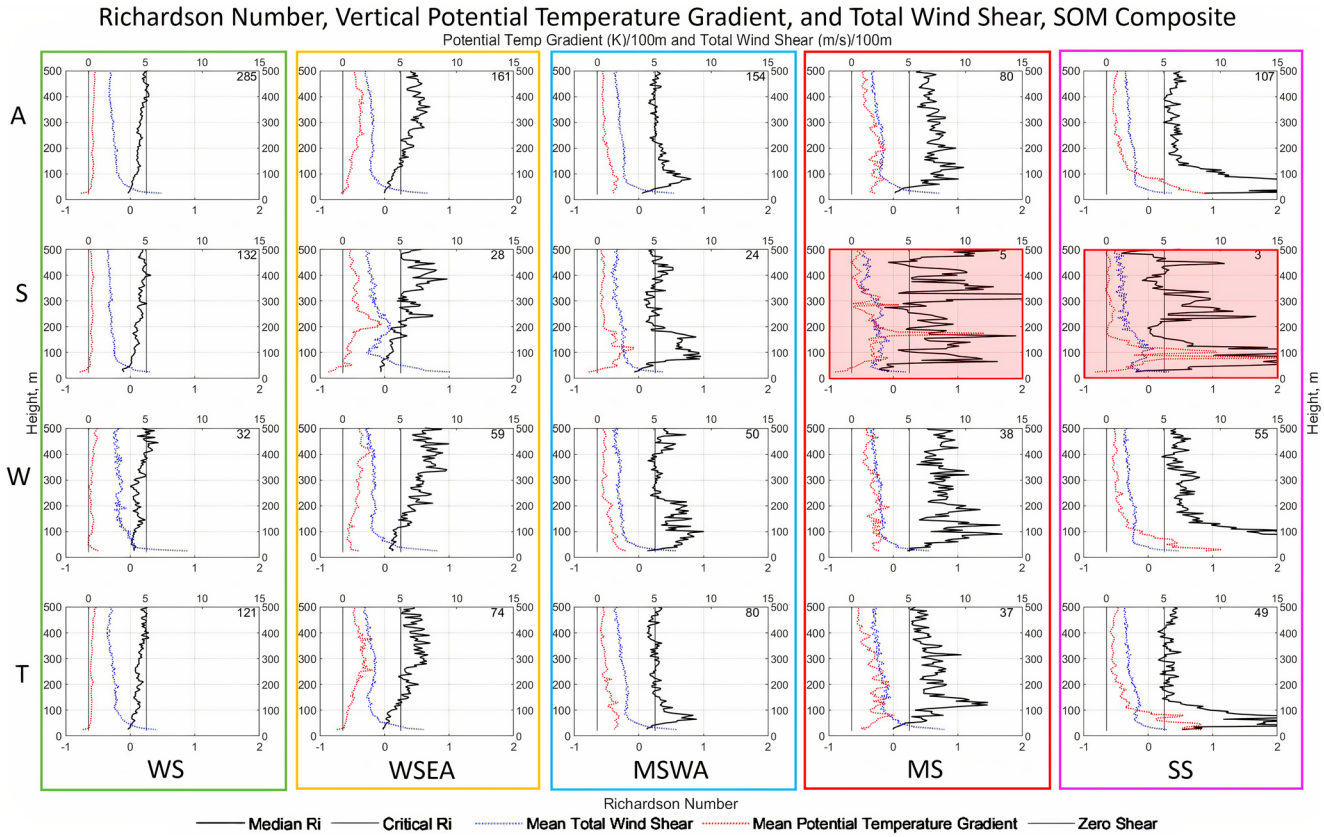

Figure 8. Richardson number median profile (solid black), mean potential temperature gradient (dotted red), and mean total wind shear (dotted blue) for each season and regime. The critical Richardson number (0.25) is also shown as a solid gray line. These values are plotted for each stability regime (WS, WSEA, MSWA, MS and SS) annually (A) (top row), and for the summer (S), winter (W), and transition (S) seasons (second through fourth rows respectively). The numbers in the top right of each profile indicate the number of radiosonde profiles mapped to each regime. Patterns with a red shade indicate that there were ten or fewer observations that mapped to that pattern. The Richardson number is associated with the bottom *x*-axis and the potential temperature gradient and total wind shear are associated with the top *x*-axis.

a smaller positive bulk Richardson number indicates weak stability and/or large wind shear. The critical bulk Richardson number indicates the point at which turbulence in the atmosphere cannot be sustained (Stull, 1988). Different values of the critical bulk Richardson number are often used (Zilitinkevich & Baklanov, 2002), usually between 0.20 and 1.0 (Galperin et al., 2007). Here we use 0.25 as the critical bulk Richardson number to serve as a guideline for qualitative assessment of turbulence in the different stability regimes being analyzed in this paper.

Figure 8 shows the composited median bulk Richardson number profile (bottom *x*-axis label), the mean total wind shear profile (top *x*-axis label), and the mean potential temperature gradient profile (top *x*-axis label), as well as the critical bulk Richardson number (0.25, bottom *x*-axis label) for each stability regime. Here we approximate the boundary layer depth as the height at which the bulk Richardson number first exceeds the critical bulk Richardson number (0.25) (Brümmer & Thiemann, 2002; Zilitinkevich & Baklanov, 2002). Generally, the median bulk Richardson number is near or below critical, indicating regions that are likely to be turbulent, over the full depth of the profile for the WS regime, in lowest 120 m in the WSEA regime, at the surface and then above 215 m in the MSWA regime, and only near the surface in the MS regime. The bulk Richardson number is above the critical value over the entire depth of the SS regime. This indicates that turbulence is intermittent or absent outside of these height ranges in each of these regimes, except immediately adjacent to the surface where wind shear is much stronger. These varying vertical distributions of Richardson numbers across the different regimes also provide guidance as to the depth of the boundary layer in each regime. The boundary layer is deepest in the WS case, extending over the entire 500 m height range shown here. The boundary layer is about 120 m in the WSEA regime and confined to the near surface layer in the MSWA, MS and SS regimes, although turbulence aloft may be present in the MSWA regime.

The results here are similar to the conclusion from Banta et al. (2007), who found that strongly stable conditions are associated with weak wind shear and large Richardson numbers. The very large shear near the surface in the MS regime in the transition seasons is associated with the strong low-level wind maximum in this case. The large wind shear near the surface in this regime reduces the Richardson number below critical near the surface, but it is not strong enough to overcome the strong stability above the surface, and thus the Richardson number remains above critical over most of the depth of the profile.

4. Summary and Future Work

In this paper, the relationships present between atmospheric state, radiative fluxes, and boundary layer stability at McMurdo Station, Antarctica were explored. In summary, it was found that:

- There is a strong seasonal cycle of the different stability regimes (Table 2)
  - Winter exhibits more variety in stability regimes than what would be expected for the polar winter, when strong stability would be expected to dominate. In winter, weaker stability regimes occur 39% of the time while moderate to strong stability regimes occur 61% of the time.
  - In summer, the WS and WSEA regimes dominate, occurring about 83% of the time while moderate to strong stability regimes (MSWA, MS and SS) occur less than 17% of the time.
  - The transition seasons largely mirror the stability regime frequencies seen annually, with WS being the most commonly observed regime (33.5%) followed by the WSEA and MSWA regimes.
- Changes in the sign of net radiation helps explain most, but not all, of the variability between weak and moderate or strong stability regimes (Figure 5).
  - The net radiation is negative in the winter and positive in the summer consistent with the dominance of moderate to strong stability in winter and weak stability in summer.
  - However, the negative net radiation across all regimes in winter, and positive net radiation across all regimes in summer suggests that other mechanisms are responsible for variations in stability during these seasons.
- Considering both net radiation (Figure 5) and near surface wind speed (Figure 6) provides additional insight into the forcing for the different stability regimes.
  - Winter boundary layer stability varies in response to changes in net radiation and wind speed. Despite negative net radiation in the WS and WSEA cases, the moderate 20 m wind speeds likely generate enough mechanical mixing to create the weak stability observed in these regimes. For the other winter regimes the negative net radiation combined with weak winds lead to moderate or strong near surface stability.
  - Summer positive net radiation and moderate winds are responsible for the occurrence of the WS and WSEA regimes. For the MSWA, MS, and SS regimes in summer, the positive net radiation and moderate 20 m wind speeds are inconsistent with moderate to strong stability. We hypothesize that differential temperature advection, possibly in response to sea ice cover just offshore from McMurdo, may lead to the infrequent formation of the moderate and strong stability regimes.
  - The transition seasons experience a change in sign of the net radiation across regimes with positive net radiation seen for WS and WSEA and negative net radiation seen for the SS regime, consistent with radiative forcing being the dominant mechanism leading to these different stability regimes.
  - The MSWA and MS regimes have a slightly positive median net radiation during the transition seasons as well as moderate wind speeds. It is possible that differential temperature advection causes these moderate stability regimes to form.
- Mean low-level wind maxima were noted in all seasons for the WSEA regime as well as in the transition seasons for the MSWA, MS and SS regimes (Figure 7)
  - LLJs occurred in more than 50% of all WSEA cases throughout the year, but were most frequent (73%) in the MS regime during the transition seasons (Table 3).
  - We hypothesize that the WSEA LLJs form as a result of winds being funneled between the terrain around McMurdo and the enhanced stability aloft
  - In contrast, we suggest that the low-level stability interacting with the terrain results in a thermal wind that leads to the formation of the LLJs in the MSWA, MS and SS regimes.

- Weak stability is associated with sub-critical bulk Richardson values and well-developed turbulence, and cases of stronger stability (MS and SS regimes) are associated with bulk Richardson values mostly above critical, which suggests intermittent turbulence in these regimes.
  - o The depth of turbulence, which defines the boundary layer depth, is deeper in the weaker stability regimes, and becomes more shallow with increasing stability.

Further, the complexities of the local terrain and impacts of the radiosonde drift distance could result in the observation of boundary layer structures not immediately associated with that at McMurdo Station, but rather above sea ice or open ocean, which can complicate the results.

Future work will assess how well the Antarctic Mesoscale Prediction System (AMPS) reproduces the different stability regimes and the relationship to other atmospheric properties and fluxes. The data from the West Antarctic Ice Sheet (WAIS) portion of the AWARE campaign, as well as from other sites with radiosonde and radiation observations, will be analyzed in the same way as the results presented here to compare boundary layer forcing mechanisms across the Antarctic continent.

Appendix A

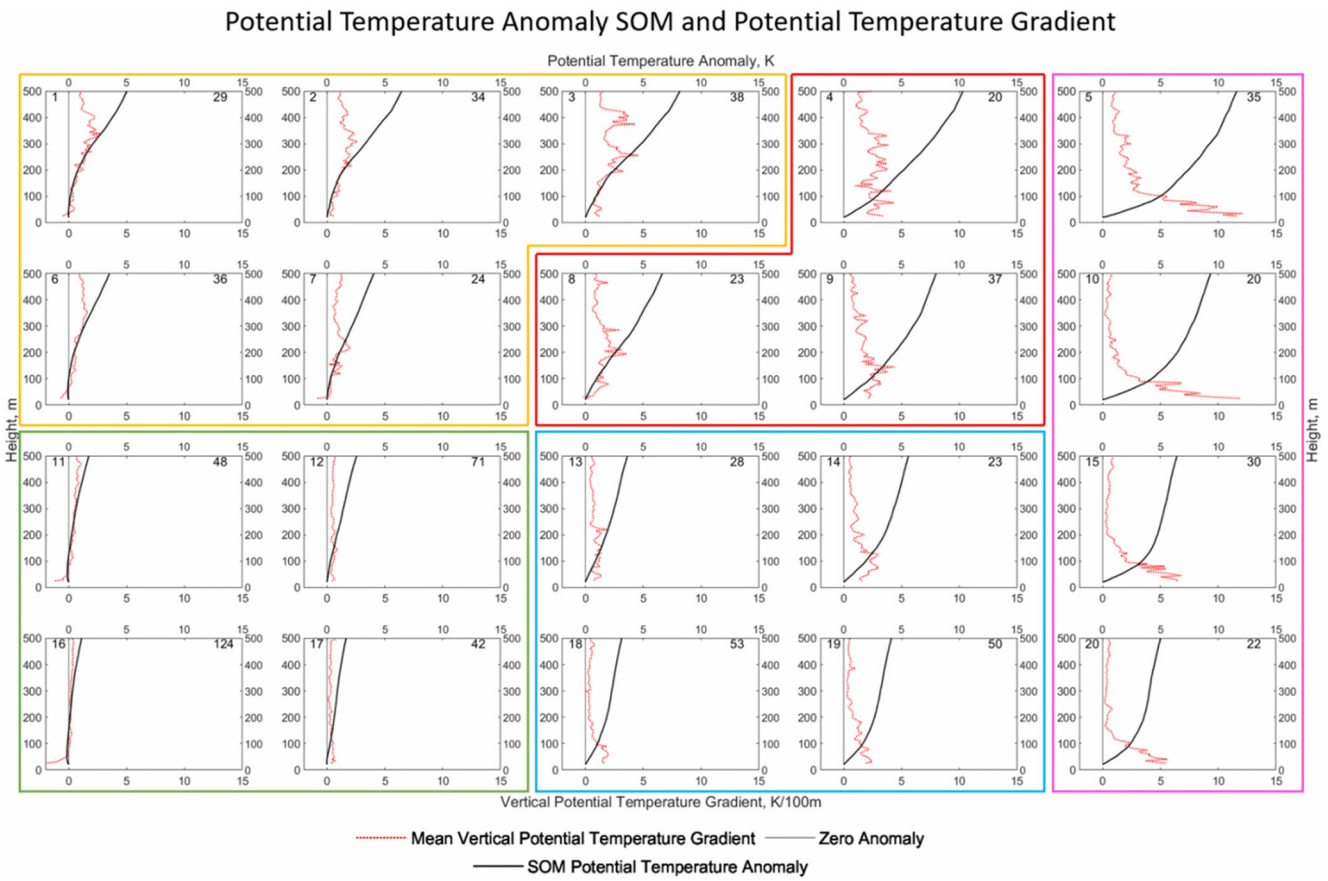

Figure A1. Potential temperature anomaly profiles from 20 to 500 m above ground level identified by the self-organizing map algorithm (black), potential temperature gradient profiles (red dotted line) and a line of zero gradient (gray). The numbers in the top right of each profile indicate the number of radiosonde profiles mapped to each regime. The numbers in the top left of each pattern is the pattern number. The colored outlines around the different SOM patterns indicate which regime the patterns correspond to: Weak Stability (WS): green, Weak Stability, Enhanced Aloft (WSEA): orange, Moderate Stability, Weak Aloft (MSWA): blue, Moderate Stability (MS): red, and Strong Stability (SS): pink (Table 2).

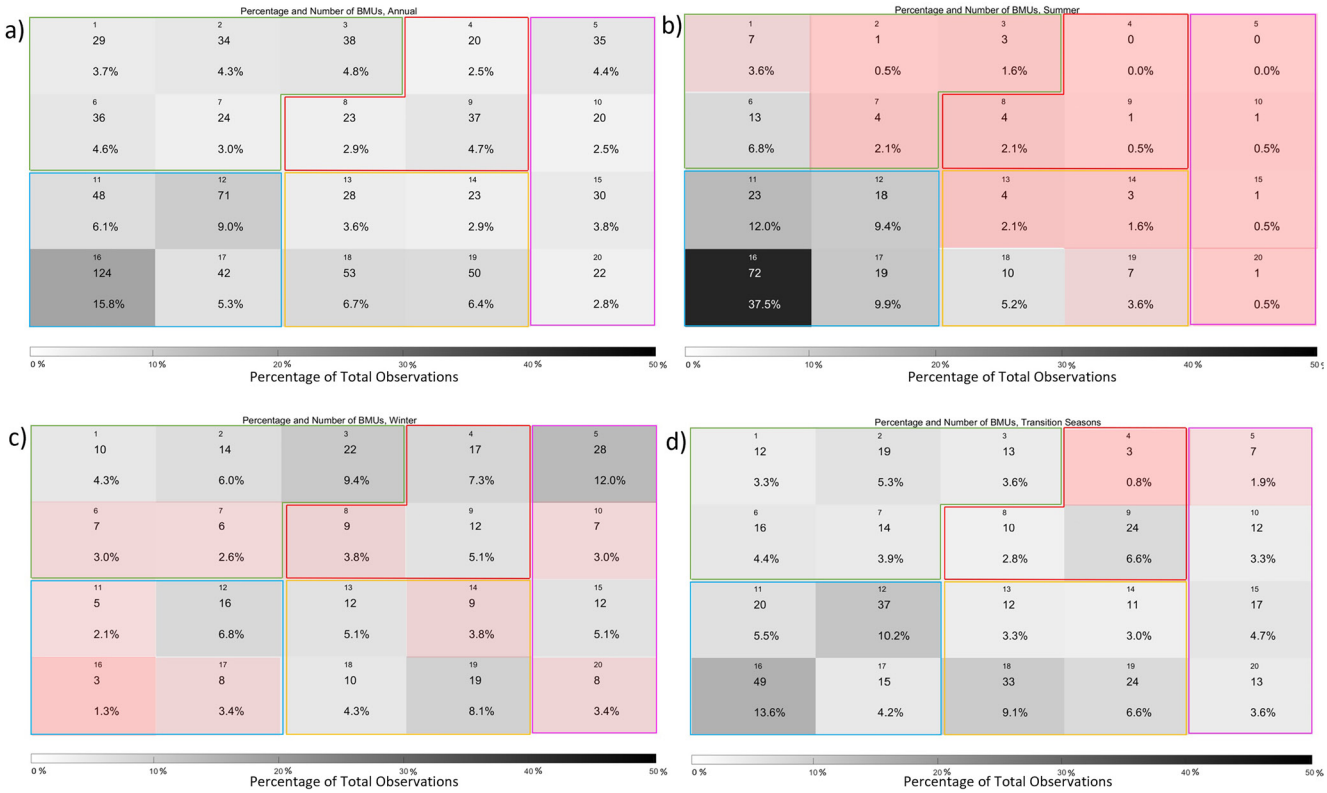

Figure A2. Number of BMUs (top large number) and frequency of occurrence (bottom large number, %) for each SOM pattern for the entire 13-month data set (a), for the summer months of December and January (b), the winter months of May, June, July, and August (c), and the transition season months of February March, April, September, October, and November (d). The SOM node number is given as a small number at the top center for each shaded box. Gray shading indicates the SOM pattern frequency of occurrence with darker shading indicating patterns that occur more frequently. Dark red shading indicates SOM patterns with fewer than 5 BMUs and light red shading indicates SOM patterns with 6–10 BMUs.

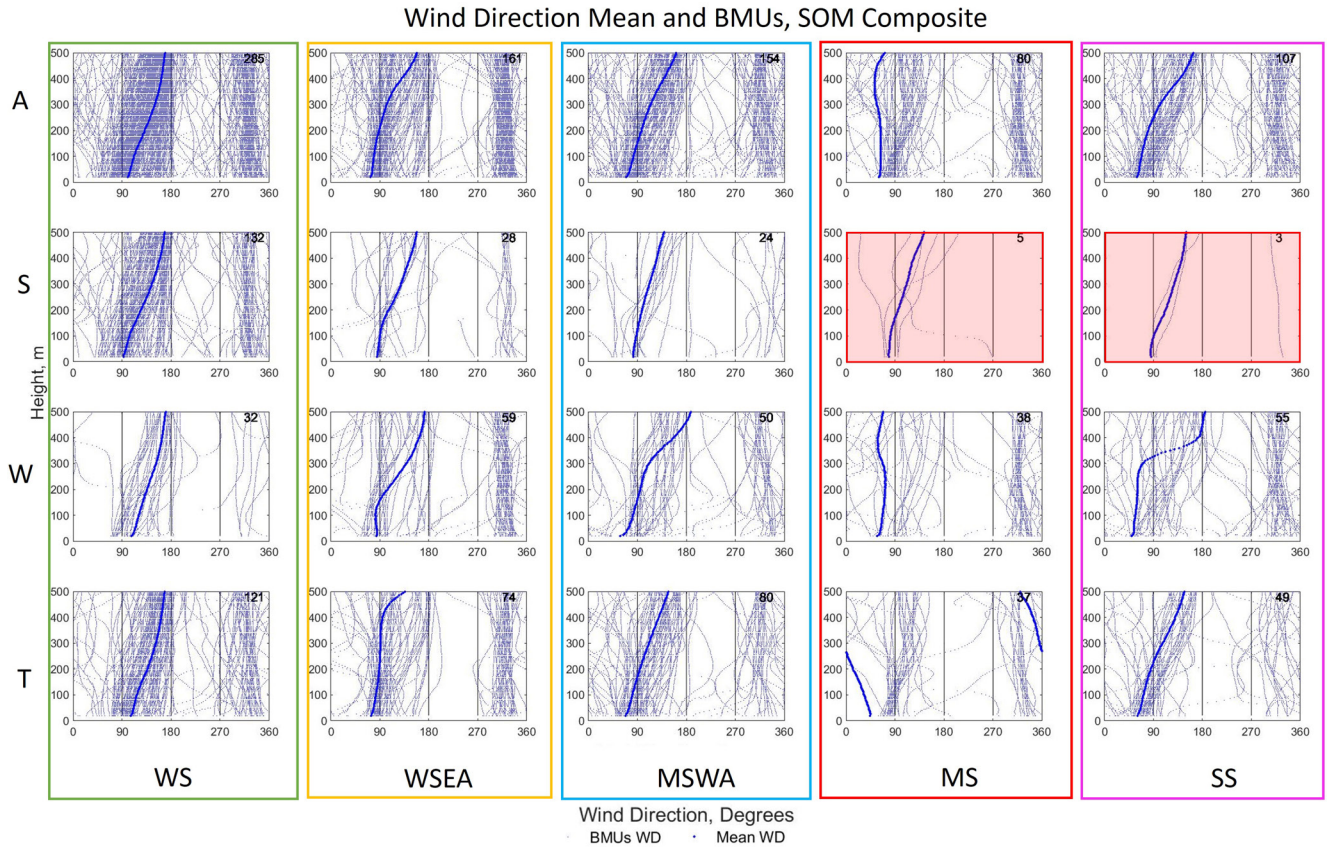

Figure A3. Mean wind direction profile (large blue stars), and the wind direction BMUs for each regime and season (small blue stars). These values are plotted for each stability regime (WS, WSEA, MSWA, MS, and SS) for annual (A) (top row), and summer (S), winter (W), and transition (T) seasons (second through fourth rows respectively). The numbers in the top right of each profile indicate the number of radiosonde profiles mapped to each regime, or the BMUs.

Data Availability Statement

The data used to support this project can be found: https://adc.arm.gov/discovery/#/results/site_code::awr.

Acknowledgments

This work was funded by the United States National Science Foundation (NSF) grant OPP 1745097. The author thanks the United States Antarctic Program and the Department of Energy for support and logistics for the data used in this paper. The authors thank two anonymous reviewers for their insightful comments and suggestions which have improved this manuscript. The author also thanks Dr. Matthew Lazzara, Dr. Jan Lenaerts, Dr. Julie Lundquist, and Dr. Mark Serreze for their valued feedback and support.

References

Andreas, E. L., Claffy, K. J., & Makshtas, A. P. (2000). Low-level atmospheric jets and inversions over the western Weddell Sea. *Boundary-Layer Meteorology*, *97*, 459–486. https://doi.org/10.1023/A:1002793831076

Baas, P., Bosveld, F. C., Klein Baltink, H., & Holtslag, A. A. M. (2009). A climatology of nocturnal low-level jets at Cabauw. *Journal of Applied Meteorology and Climatology*, *48*, 1627–1642. https://doi.org/10.1175/2009JAMC1965.1

Banta, R. M., Mahrt, L., Vickers, D., Sun, J., Balsey, B. B., Pichugina, Y. L., & Williams, E. J. (2007). The very stable boundary layer on nights with weak low-level jets. *Journal of the Atmospheric Sciences*, *64*(9), 3068–3090. https://doi.org/10.1175/JAS4002.1

Bonner, W. D. (1968). Climatology of the low level jet. *Monthly Weather Review*, *96*, 833–850. https://doi.org/10.1175/1520-0493(1968)096<0833:cotllj>2.0.co;2

Brümmer, B., & Thiemann, S. (2002). The atmospheric boundary layer in an arctic wintertime on-ice air flow. *Boundary-Layer Meteorology*, *104*, 53–72.

Carroll, B. J., Demoz, B. B., & Delgado, R. (2019). An overview of low-level jet winds and corresponding mixed layer depths during PECAN. *Journal of Geophysical Research: Atmospheres*, *124*, 9141–9160. https://doi.org/10.1029/2019JD030658

Cassano, E. N., Glisan, J. M., Cassano, J. J., Gutowski Jr., W. J., & Seefeldt, M. W. (2015). Self-organizing map analysis of widespread temperature extremes in Alaska and Canada. *Climate Research*, *62*, 199–218. https://doi.org/10.3354/cr01274

Cassano, J. J., Nigro, M., & Lazzara, M., (2016). Characteristics of the near surface atmosphere over the Ross ice shelf, Antarctica. *Journal of Geophysical Research: Atmospheres*, *121*, 3339–3362. https://doi.org/10.1002/2015JD024383

Chenge, Y., & Brutsaert, W. (2005). Flux-profile relationships for wind speed and temperature in the stable atmospheric boundary layer. *Boundary-Layer Meteorology*, *114*, 519–538. https://doi.org/10.1007/s10546-004-1425-4

Comiso, J. C. (1994). Surface temperatures in the polar regions from Nimbus 7 temperature humidity infrared radiometer. *Journal of Geophysical Research*, *99*, 5181–5200. https://doi.org/10.1029/93JC03450

Galperin, B., Sukoriansky, S., & Anderson, P. S. (2007). On the critical Richardson number in stably stratified turbulence. *Atmospheric Science Letters*, *8*, 65–69. https://doi.org/10.1002/asl.153

Hudson, S., & Brandt, R. (2005). A look at the surface-based temperature inversion on the Antarctic Plateau. *Journal of Climate*, *18*, 1673–1696. https://doi.org/10.1175/JCLI3360.1

Jakobson, L., Vihma, T., Jakobson, E., Palo, T., & Jaagus, J. (2013). Low-level jet characteristics over the Arctic Ocean in spring and summer. *Atmospheric Chemistry and Physics*, *13*, 11089–11099. https://doi.org/10.5194/acp-13-11089-2013

King, J. C., & Turner, J. (1997). *Antarctic Meteorology and Climatology, Cambridge Atmospheric and Space Sciences Series*, Cambridge University Press.

Lawrence, D. A., & Balsley, B. B. (2013). High-resolution atmospheric sensing of multiple atmospheric variables using the DataHawk small airborne measurement system. *Journal of Atmospheric and Oceanic Technology*, *30*, 2352–2366. https://doi.org/10.1175/JTECH-D-12-00089.1

Lubin, D., Bromwich, D. H., Vogelmann, A. M., Verlinde, J., & Russell, L. M. (2017). ARM West Antarctic Radiation Experiment (AWARE) Field Campaign Report, DOE/SC-ARM-17-028.

Lubin, D., Zhang, D., Silber, I., Scott, R. C., Kalogeras, P., Battaglia, A., et al. (2020). AWARE: The atmospheric radiation measurement (ARM) west Antarctic radiation experiment. *Bulletin of the American Meteorological Society*, *101*, E1069–E1091. https://doi.org/10.1175/BAMS-D-18-0278.1

Matsuoka, K., Skoglund, A., & Roth, G. (2018). Quantarctica [data set]. Norwegian Polar Institute. https://doi.org/10.21334/npolar.2018.8516e961

Nigro, M. A., Cassano, J. J., Wille, J., Bromwich, D. H., & Lazzara, M. A. (2017). A self-organizing-map-based evaluation of the Antarctic mesoscale prediction system using observations from a 30-m instrumented tower on the Ross ice shelf, Antarctica. *Weather and Forecasting*, *32*, 223–242. https://doi.org/10.1175/WAF-D-16-0084.1

Parish, T. R. (2017). On the forcing of the summertime great plains low-level jet. *Journal of the Atmospheric Sciences*, *74*, 3937–3953. https://doi.org/10.1175/JAS-D-17-0059.1

Phillpot, H. R., & Zillman, J. W. (1970). The surface temperature inversion over the Antarctic continent. *Journal of Geophysical Research*, *75*, 4161–4169. https://doi.org/10.1029/JC075i021p04161

Riordan, A. J. (1977). Variations of temperature and air motion in the 0- to 32-meter layer at Plateau Station, Antarctica. *Meteorological Studies at Plateau Station, Antarctica, Antarctic Research Series*, edited by In J. A. Businger (Ed.),. AGU.

Rodrigo, J. S., & Anderson, P. S. (2013). Investigation of the stable atmospheric boundary layer at Halley Antarctica. *Boundary-Layer Meteorology*, *148*, 517–539. https://doi.org/10.1007/s10546-013-9831-0

Schwartz, B. E., & Doswell III, C. A. (1991). North American rawinsonde observations: Problems, concerns, and a call to action. *Bulletin of the American Meteorology Society*, *72*, 1885–1896. https://doi.org/10.1175/1520-0477(1991)072<1885:naropc>2.0.co

Seefeldt, M. W., Tripoli, G. J., & Stearns, C. R. (2003). A high-resolution numerical simulation of the wind flow in the Ross Island Region, Antarctica. *Monthly Weather Review*, *131*, 435–458. https://doi.org/10.1175/1520-0493(2003)131<0435:ahrnso>2.0.co;2

Silber, I., Verlinde, J., Eloranta, E. W., & Cadeddu, M. (2018). Antarctic Cloud macrophysical, thermodynamic phase, and atmospheric inversion coupling properties at McMurdo station: I. Principal data processing and climatology. *Antarctic cloud macrophysical, thermodynamic phase, and atmospheric inversion coupling properties at McMurdo Station: I. Principal data processing and climatology, United States*, *123*, 6099–6121. https://doi.org/10.1029/2018JD028279

Stull, R. B. (1988). *An Introduction to Boundary Layer Meteorology*, Springer.

Tuononen, M., Sinclair, V. A., & Vihma, T. (2015). A climatology of low-level jets in the mid-latitudes and polar regions of the Northern Hemisphere. *Atmospheric Science Letters*, *16*, 492–499. https://doi.org/10.1002/asl.587

Xu, M., Li, Y., Yang, Q., Gao, A. E., Han, B., Yang, Y., et al. (2019). Radiosonde-observed vertical profiles and increasing trends of temperature and humidity during 2005–2018 at the South Pole. *Atmosphere*, *10*, 365–381. https://doi.org/10.3390/atmos10070365

Zhang, Y., Seidel, D., Golaz, J., Deser, C., & Tomas, R. (2011). Climatological characteristics of Arctic and Antarctic surface-based inversions. *Journal of Climate*, *24*, 5167–5186. https://doi.org/10.1175/2011JCLI4004.1

Zilitinkevich, S., & Baklanov, A. (2002). Calculation of the height of the stable boundary layer in practical applications. *Boundary-Layer Meteorology*, *105*, 389–409. https://doi.org/10.1023/A:1020376832738